Strengthening Aluminum by Zirconium and Chromium

by

Shi Yan

A Thesis

Submitted to the Faculty of the

WORCESTER POLYTECHNIC INSTITUTE

in partial fulfillment of the requirements for the

Degree of Master of Science

in

Materials Science and Engineering

December 2012

APPROVED:

Dr. Makhlouf M. Makhlouf, Major Advisor

_____

Dr. Richard D. Sisson, Jr., Director of Manufacturing and Materials Engineering

_____

Abstract

The Al-Zr system is used to form a thermally stable strengthening phase in high temperature aluminum-base casting alloys. These alloys have good strength at elevated temperature due to the precipitation of coherent metastable Al_3Zr particles upon decomposition of the supersaturated Al-Zr solid solution by a carefully designed heat treatment. Formation of the Al_3Zr particles occurs by a peritectic reaction, which decrees that once formed, the particles cannot be dissolved by a solid-state homogenization process. Accordingly, melting the alloy must serve as the homogenization step of the precipitation hardening process; and solidification during casting must serve as the quenching step. Unfortunately, a prohibitively fast solidification rate is necessary to obtain a solid solution with as little as 0.4% Zr in Al. It is found that adding Cr to Al-0.4wt%Zr binary alloy makes it easier to form the supersaturated solid solution, and the ternary Al-0.4wt%Zr-0.8wt%Cr alloy has better room and elevated temperature tensile properties than the binary Al-0.4wt%Zr alloy. Various one-step and two-step isothermal aging cycles were investigated in order to arrive at the optimum aging schedule for the Al-0.4wt%Zr-0.8wt%Cr. It is found that soaking the alloy at 400°C for 24 hours is optimum; and employing a two-step aging schedule reduces the aging time without sacrificing strength. The two-step aging schedule includes soaking the alloy at 375°C for 3 hours and then at 425°C for an additional 12 hours. Examination of the precipitates that form in the Al-0.4wt%Zr-0.8wt%Cr with High Resolution Transmission Electron Microscopy (HRTEM) shows that they have the $L1_2$ crystal structure. Energy Dispersive Spectrometry (EDS) shows that the particles contain only aluminum and zirconium whereas the matrix is a solid solution of chromium in aluminum. Hence, it is suggested that zirconium strengthens the Al-0.4wt%Zr-0.8wt%Cr alloy by a precipitation hardening mechanism and chromium further enhances the strength by solid solution strengthening.

Acknowledgments

This research could not be completed without the support of many individuals. Their contribution in various ways to my work deserves special mention. It is a pleasure to convey my gratitude to them all in humble.

First and foremost, I thank my advisor Professor Makhlouf M. Makhlouf for giving me the opportunity to work with him. It has been an honor to be his student. I like to deliver my special gratitude to him for sharing his invaluable insight, advice and knowledge with me. His words of encouragement and motivation came a long way in bringing this work to completion. I like to thank my thesis committee, Professor Richard D. Sisson Jr., Professor Jianyu Liang, and Dr. Libo Wang for their time and assistance in this work. Thanks to Dr. Boquan Li for assistance with TEM work. I also give a very special thanks to Yangyang Fan and Lance Wu for help all through this work. It is my pleasure also to pay tribute to all the WPI faculty and staff.

I like to express my great gratitude to my parents, without their never-ending love, understanding and support, this thesis would be impossible. Collective and individual acknowledgements are also due to my colleagues, classmates and friends whose enthusiasm and support in one way or another was helpful and memorable.

I thank the Department of Materials Science and Engineering at WPI and Metal Processing Institute for giving me the opportunity to be a part of them. Finally, I thank everyone who supported and believed in me, and I express my apology to anyone who I did not mention personally.

Table of Contents

List of Tables

List of Figures

1. Objectives

The objectives of this thesis are as follows:

(1) To develop an Al-Zr-Cr alloy that can be conventionally cast and that is suitable for use in elevated temperature applications.

(2) To elucidate the strengthening mechanism(s) operative in Al-Zr-Cr alloys.

(3) To investigate the effect of Cr on (i) the chemical constitution, (ii) the crystal structure, and (iii) the mean radius and coherency of the precipitate particles that form in the Al-Zr-Cr alloy when it is optimally heat-treated.

2. Background

It is well known that the number and motion of dislocations present in an alloy control its strength. The stress required to move the dislocations, known as the Peierls-Nabarro stress, is quite low in pure metals; consequently, pure metals are week. In order to make pure metals stronger, one must restrict the motion of their dislocations by either creating internal stresses that oppose dislocation motion, or by placing obstacles in the path of dislocations that force them to either loop around them or cut through them. There are three different strengthening mechanisms that may be operative in aluminum casting alloys, and they are discussed in the following sections.

2.1 Strengthening by Grain Size Reduction

It has been observed that there is a strong relationship between the grain size of a metal and its strength: The smaller the grain size, the higher the strength. The increase in tensile yield strength of a metal caused by reducing its grain size may be described by the Hall-Petch [1, 2] relation shown as Eq. (1),

$$\sigma = \sigma_o + \frac{k}{\sqrt{d}} \tag{1}$$

In Eq. (1), σ_o and k are constants obtained from linear fitting of measured data and d is the average grain diameter. Many models have been proposed to explain the experimentally observed Hall-Petch effect. Some models attribute the Hall-Petch strengthening to dislocation pileups against grain boundaries, which lead to a concentration of stress at the boundary. As the stress concentration increases to a critical level, yielding starts in the adjacent grain. Large grains have a smaller number of dislocations piled-up at their boundaries, and therefore they have a reduced stress concentration in their next grains and a lower yield stress than smaller grains. On the other hand, the Dislocation Density models assume that the Hall-Petch strengthening is due to two contributions: One contribution is from statistically stored dislocations, and the other is from geometrically necessary

dislocations. The former is grain size independent while the latter depends on grain size, which decreases as the average grain diameter increases.

Compared with other metals, the grain size strengthening effect in aluminum is small. As Table 1 shows, the Hall-Petch constant k of pure aluminum is much smaller than that of other metals such as titanium and iron.

Table 1. The Hall-Petch constants of some common metals [3].

Metal	k (MPa. mm$^{1/2}$)
Aluminum	2.16
Titanium	12.75
Iron	18.44
Copper	3.53

2.2 Strengthening by Forming Solid Solutions

The addition of foreign atoms to a pure metal invariably increases the strength of the metal because the solute atoms make it harder for dislocations to move. Depending on the size of the solute atoms, a substitutional solid solution or an interstitial solid solution can form. In both solid solutions, the overall crystal structure remains unchanged. In aluminum alloys, solute atoms usually substitute the aluminum atoms. The strengthening effect of solute atoms has been investigated by many researchers over the years, and several mechanisms have been proposed. All these mechanisms relate the increase in strength to a numbers of different interactions that occur between dislocations and the solute atoms. These interactions are influenced by two factors that are known as (i) the size effect and (ii) the modulus effect. The former is caused by the difference in size between the solute and solvent atoms, which creates a strain field in the lattice; and the latter is caused by the difference in shear modulus between the solute and the lattice atoms, which results in a hard or soft “spot” in the matrix.

2.3 Strengthening by Forming Precipitate Particles

Essentially, precipitation strengthening is achieved by producing in the alloy's matrix a particulate dispersion of obstacles that impede the movement of dislocations. The extent of strengthening that results depends largely on the metallic system involved, the volume fraction and average size of the dispersed particles, and the nature of the interaction between the precipitate particles and dislocations. The type of interaction between the precipitate particles and dislocations dictates the magnitude of the strengthening increment. There are two main types of particle-dislocation interactions. They are:

Particle Looping – The shear stress required for a dislocation to loop around a precipitate particle is inversely proportional to the edge-to-edge distance between the particles, which was first described by Orowan [4] as shown in Eq. (2)

$$\Delta\tau_y \propto \frac{Gb}{L} \tag{2}$$

This leads to the increase in the tensile yield strength [5] of the metal given by Eq. (3),

$$\Delta\sigma_{or} = M \cdot \frac{0.4Gb}{\pi\sqrt{(1-\nu)}} \cdot \frac{\ln(\frac{2\bar{R}}{b})}{\lambda} \tag{3}$$

In Eq. (3), M is the Taylor Factor, G and ν are the shear modulus and Poisson ratio of the matrix, b is the magnitude of the Burgers Vector, $\bar{R}$ is the mean planar precipitate radius (not equal to the mean radius, $<R>$), and λ is an effective inter-precipitate distance, which takes into account the finite size of the precipitates. Both $\bar{R}$ and λ depend on the distribution of precipitate sizes. For a mono-dispersed assembly of particles, these parameters are given by Eqs. (4 and 5) [6, 7, 8]:

$$\bar{R} = \frac{\pi}{4} < R > \tag{4}$$

$$\lambda = (\sqrt{\frac{2\pi}{3f}} - 2\frac{\pi}{4}) < R > \quad (5)$$

In Eq. (5), f is the volume fraction of precipitate particles.

Particle Cutting – When the average diameter of the particles is very small, the applied shear stress on each particle becomes very large and the dislocations may be able to shear the precipitate particles. This process is described by the Anti-Phase Boundary (APB) mechanism [9] where the strengthening increment, $\Delta\sigma_{APB}$, may be calculated with Eq. (6),

$$\Delta\sigma_{APB} = M\frac{(\gamma_{APB})^{\frac{3}{2}}}{b^2}\sqrt{\frac{rf}{G}} \quad (6)$$

In Eq. (6), γ_{APB} is the antiphase boundary energy, r is the average radius of the particles and f is their volume fraction.

2.4 Kinetics of Precipitate Coarsening

Thermal stability of the alloy depends to a large extent on the size and distribution of the precipitate particles. Therefore, it is necessary to review the coarsening kinetics of precipitates. The diffusion-limited precipitate coarsening model for binary alloys was developed by Lifshitz, Slyozov and Wagner [10, 11]. This model is now referred to as the LSW model. The LSW model assumes that: (i) the linearized version of the Gibbs-Thomson equation is valid; (ii) no elastic interactions occur among the precipitates, thereby limiting the precipitate volume fraction to zero; (iii) the diffusion fields of the precipitate particles do not overlap; (iv) dilute solution theory obtains; (v) coarsening occurs in a stress-free matrix; (vi) precipitates have a spherical morphology; (vii) precipitates form with the correct composition as given by the equilibrium phase diagram; and (viii) coarsening is a self similar process [12, 13]. The LSW model shows that the average precipitate size <R> increases with time according to Eq. (6),

$$< R(t) >^3 - < R(t=0) >^3 = kt \quad (6)$$

In Eq. (6), <R (t)> is the average precipitate radius at time t, <R (t = 0)> is the average precipitate radius at the onset of coarsening, and k is the coarsening rate given by [14]:

$$k \propto \frac{D\sigma}{(C_e^{\beta} - C_e^{\alpha})^2} \tag{7}$$

In Eq. (7), D is the diffusivity of the rate-controlling solute, σ is the precipitate-matrix interfacial free energy, and C_e^{β} and C_e^{α} are the equilibrium solubilities of the solute elements in the precipitate and matrix phases, respectively. Based on Eqs. (6) and (7), a creep-resistant aluminum alloy, the solutes should have limited diffusivity in the aluminum matrix and it is essential to form precipitates that have a small interfacial energy with the aluminum matrix.

2.5 Principles of Developing Aluminum Alloys with High Temperature Stability and Strength

Developing aluminum alloys for elevated temperature applications has been an active field of research for several decades. There are currently two commercial alloy systems that are usable at elevated-temperatures: the Al-Zn-Cu-Mg (7xxx series) system, and the Al-Cu-Mg system (2xxx series). In these alloys, small meta-stable coherent precipitates form upon aging at temperatures below 200°C. Beside these precipitates, two other phases may contribute to the strength of these alloys. These are (a) incoherent dispersions, and (b) large particles. Incoherent dispersions are intermetallics that form by the introduction of Cr, Mn, and Ti into the alloys. The large particles are present due to the presence of Fe and Si as impurities in the alloys. The different strengthening phases make heat-treating these alloys complicated. The dispersions and inclusions are stable near the melting temperature of the alloys while the precipitates coarsen quickly and dissolve at temperatures above 300°C. Rapidly-solidified alloys based on the Al-Fe system also exhibit good performance at elevated temperatures. However, the

microstructures characteristics necessary for strength and thermal stability are formed only by rapid solidification. Unfortunately, the high cost of rapid solidification processing (RSP) limits its use in commercial applications.

Based on the behavior of modern Ni-based super alloys and considering the general requirements, Knipling [15] developed the following criteria for the selection of alloying elements capable of producing castable, precipitation-strengthened, thermally-stable aluminum-based alloys. These are:

(i) Solid-state precipitation upon aging of coherent trialuminide particles of the chemical formula Al_3M that have the $L1_2$ crystal structure so as to promote high strength and negligible coarsening at high temperature;

(ii) Shallow α-Al solvus curve to maximize the volume fraction of precipitated Al_3M particles; and the concomitant low solid solubility of these particles at the aging temperature in order to minimize particle coarsening (Eq. (6));

(iii) Low diffusivity of the alloying element (M) in aluminum in order to minimize particle coarsening and the associated loss of strength;

(iv) Solid-liquid partition coefficient (k_0) near unity in order to minimize segregation and accommodate conventional solidification

The Al-Zr system satisfies these requirements with the added benefit of low cost.

2.6 Zirconium-Containing Aluminum Alloys

Stable and meta-stable crystal structures of Al_3Zr – Zirconium is usually used as a recrystallization inhibitor and grain refiner in commercial aluminum alloys. However, even very small additions of Zr could produce a significant precipitation hardening response. This is due to the precipitation of Al_3Zr meta-stable particles with the $L1_2$ structure during post-solidification aging. The Al_3Zr meta-stable phase has the same structure as the aluminum matrix. The coherency of the meta-stable Al_3Zr particles with the aluminum matrix leads to better thermal

stability and an appreciable precipitation hardening effect. When the alloy is over-aged at high temperatures (usually above 500°C), the $L1_2$ structure transforms into the complex tetragonal DO_{23} stable structure [16, 17]. Both structures are shown schematically in Fig. 1. The DO_{23} structure precipitates are semi-coherent with the aluminum matrix. The loss in coherency accelerates the coarsening kinetics (Eq.6).

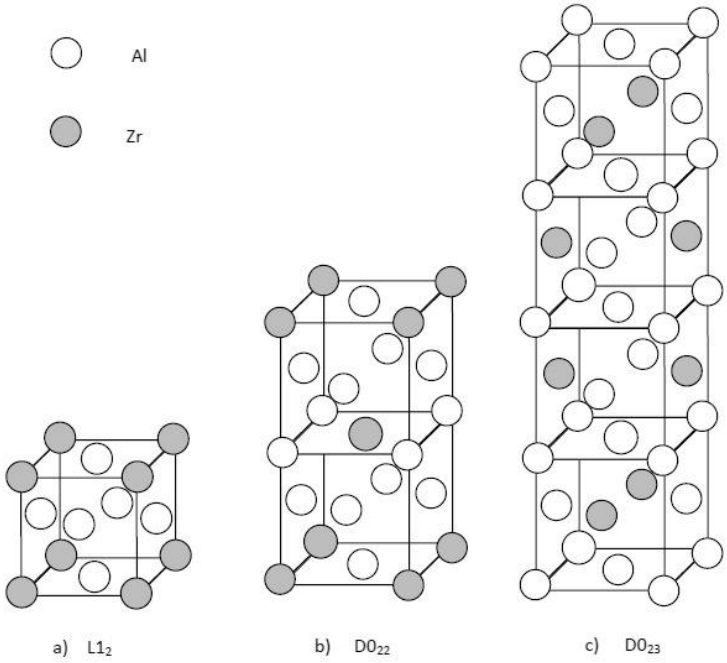

Fig. 1 $L1_2$, DO_{22} and DO_{23} crystal structures.

The diffusivity of transition metals in aluminum – Table 2 shows diffusion data for various transition metals in aluminum. The diffusion coefficient of Zr in aluminum is much smaller than that of Cu. Accordingly, Al_3Zr precipitates with the $L1_2$ crystal structure are more thermally stable than θ'-Al_2Cu precipitates.

Table 2 Diffusion data for various transition metals in aluminum [15].

Element	D_o $(\mathrm{m}^2\mathrm{s}^{-1})$	Q $(\mathrm{kJ.mol}^{-1})$	D at 400°C $(\mathrm{m}^2\mathrm{s}^{-1})$
Al	1.37×10^{-5}	124	3.25×10^{-15}
Sc	5.31×10^{-4}	173	1.98×10^{-17}
Ti	1.12×10^{-1}	260	7.39×10^{-22}
V	1.60	303	4.85×10^{-24}
Cr	10.0	281	1.29×10^{-21}
Mn	8.7×10^{-3}	208	6.24×10^{-19}
Fe	7.7×10^{-1}	221	5.41×10^{-18}
Cu	6.54×10^{-5}	136	1.54×10^{-15}
Zn	2.59×10^{-5}	121	1.05×10^{-14}
Zr	7.28×10^{-2}	242	1.20×10^{-20}
Hf	1.07×10^{-2}	241	2.11×10^{-21}

The Al-Zr phase diagram – The Al-Zr equilibrium phase diagram is shown in Fig. 2. The maximum solubility of Zr in α-Al is 0.28wt% at 667°C. And the solubility at the typical aging temperature (400°C) is negligible. The shallow α-Al solvus is helpful to maximize the volume fraction of precipitates that form in the binary alloy. And the small solubility in α-Al at the aging temperature retards the coarsening of the coherent precipitates (Eq.6). Moreover, the diffusivity of Zr in α-Al is very low ($1.2\times10^{-20}\mathrm{m}^2\mathrm{s}^{-1}$), which also minimizes coarsening of the meta-stable precipitates and the associated loss of strength.

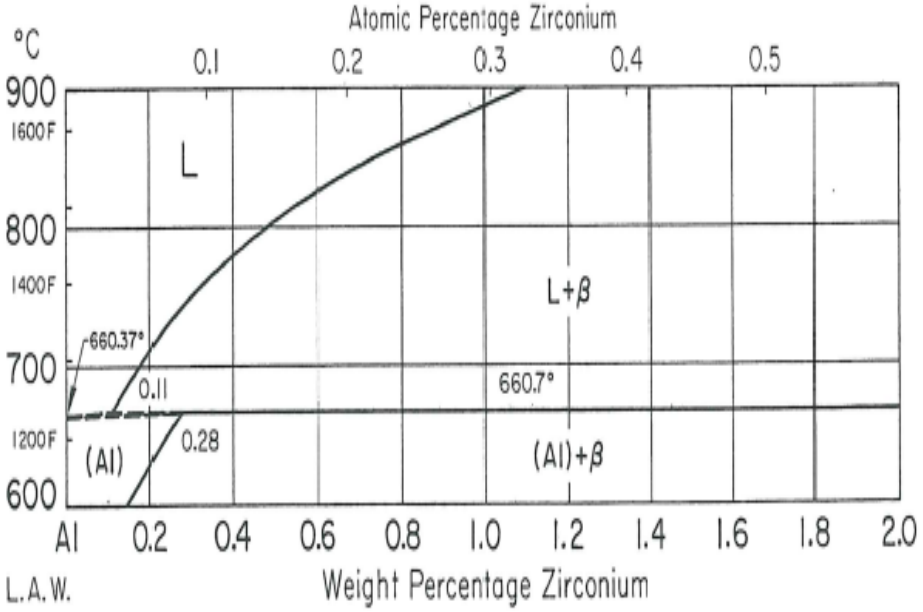

Fig. 2 The Al-rich side of the Al-Zr equilibrium phase diagram [18].

Alloying Al_3Zr with other transition metals – The small solubility of Zr in α-Al helps to retard precipitate coarsening; however, it also limits the strengthening obtained by precipitation hardening. In modern Ni-based superalloys, which are considered by many to be the most complex and successfully engineered high-temperature alloys, the solubility in Ni of the γ'-producing Al is substantial, thus allowing for a large volume fraction of precipitates to form which, in many commercial Ni base superalloys exceeds 0.7. In order to increase the volume fraction of precipitate particles in Al-Zr alloys, other elements that can form $L1_2$ Al_3M trialuminides are added with the hope that they coprecipitate with Al and Zr to form $Al_3(Zr_xM_{1-x})$. Table 3 gives examples of these elements. Besides increasing the volume fraction of the $L1_2$ precipitate, adding these elements to Al and Zr can decrease the misfit between the Al_3Zr precipitates and the α-Al matrix, which enhances the thermal stability of the precipitate. Table 4 shows the lattice parameters and the lattice mismatch between some transition metals that form $L1_2$ trialuminides and aluminum.

Table 3 Alloying Al_3Zr with other elements.

Phase	Alloying elements	References
Al_3Zr	V	[19 - 21]
	Ti	[22, 23]
	Er	[24]
	Sc	[25 - 32]
	Sc, Hf	[33]

Table 4 Lattice parameters and lattice mismatch for some $L1_2$ Al_3M trialuminides [15].

Phase	Lattice parameters (nm)	Mismatch with Al	Absolute mismatch
Group 3 transition elements			
Al_3Sc	0.4103	+1.32%	1.32%
Al_3Y	0.4234	+4.55%	4.55%
Group 4 transition elements			
Al_3Ti	0.4048	-2.04%	2.04%
Al_3Zr	0.4080	+0.75%	0.75%
Al_3Hf	0.4048	-0.04%	0.04%
Group 5 transition elements			
Al_3V	0.3870	-4.44%	4.44%
Al_3Nb	0.4110	+1.49%	1.49%
Lanthanide series (rare earth)			
Al_3Er	0.4215	+4.08%	4.08%

Alloying Al-Zr alloys with transition elements that do not form $L1_2$ Al_3M trialuminides may be a viable way of increasing the strength of Al-Zr alloys. Trialuminide particles formed by these elements, however, are not thermally stabile. Nevertheless, addition of Cr, Mn, and Fe to Al-Zr binary alloys have been shown to increase the stability of the cubic $L1_2$ structures [34- 36] that form.

The Al-Cr and Al-Cr-Zr systems – As Fig. 3 shows, compared to the Al-Zr system, the Al-Cr system has a shallower liquidus, which results in a smaller undercooling that obviates formation of the primary trialuminide phase during quenching. Consequently, it is easier to form a meta-stable supersaturated solid solution in the Al-Cr system than in the Al-Zr system. However, due to the low diffusivity of Cr in the aluminum matrix, it is very difficult for Cr to precipitate out of this super saturated solid solution. Usually, precipitation in dilute Al-Cr alloys occurs at temperatures that are higher than 500°C [37].

Fig. 4 shows the Al-rich side of the isothermal ternary Al-Cr-Zr equilibrium phase diagram at 450°C. From Fig. 4 it is clear that two phases exist in dilute Al-Cr-Zr alloys and only a small quantity of Cr and Zr dissolves in Al at this temperature. This supports the findings that adding Cr to the Al-Zr alloy increases the thermal stability of the precipitates that form [34-36]. Beside this, alloying with Cr has also been found to lead to considerable solid solution strengthening [38]. However, most of this research was performed with rapidly solidified alloys [38] and mechanically alloyed materials [34]. Moreover they do not attempt to explain how the adding Cr to Al-Zr alloys affects the crystal structure and coherency of the precipitates that form during post-solidification aging.

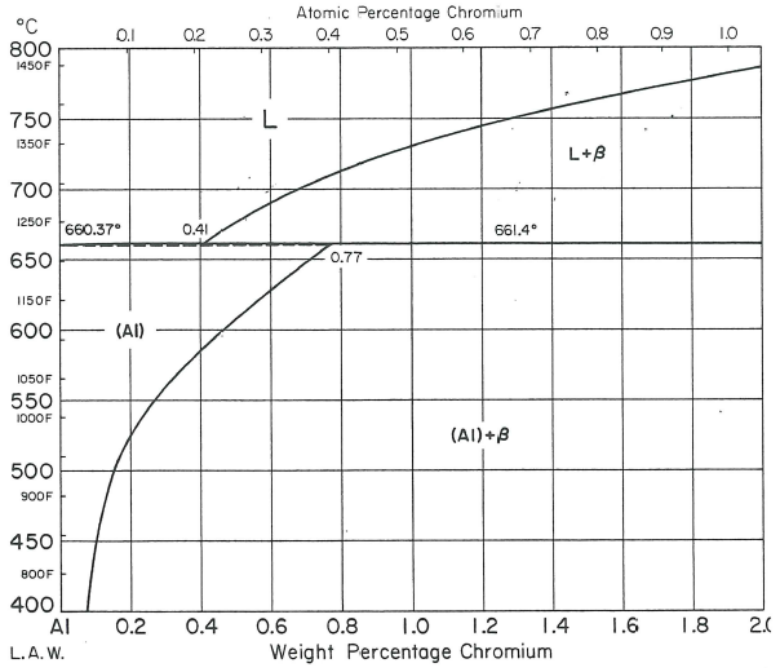

Fig. 3 The Al-rich side of the Al-Cr equilibrium phase diagram [39].

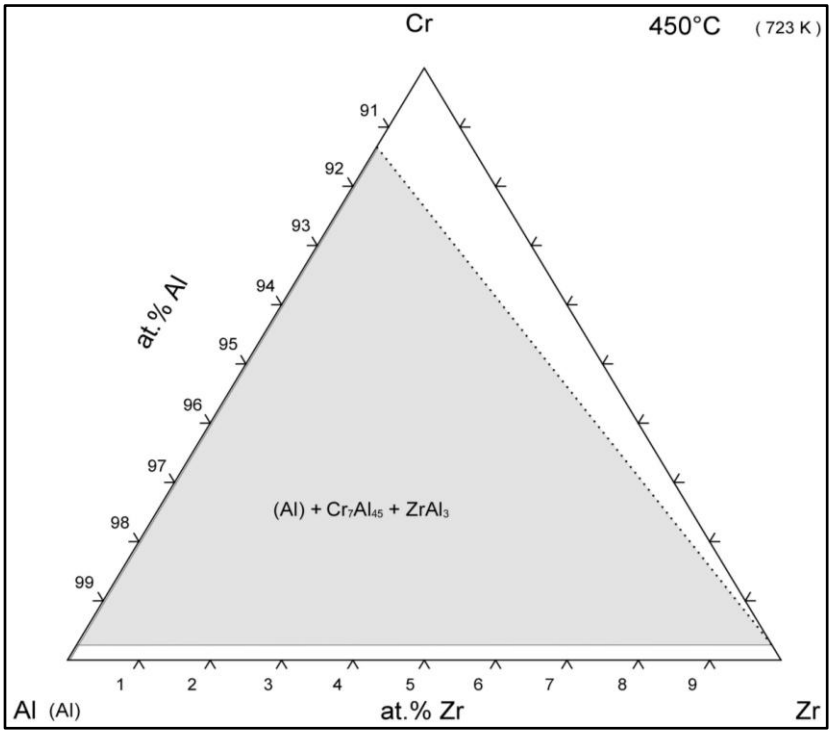

Fig. 4 The Al-rich side of the isothermal ternary Al-Cr-Zr phase diagram at 450°C [40].

3. Materials, Procedures, and Measurements

The chemical composition of the alloy is shown in Table 5 and it was prepared by induction melting[1].

Table 5 Chemical composition of the alloy.

Cr	Zr	Al
-	0.4	Remainder
0.8	-	Remainder
0.4	0.4	Remainder
0.8	0.4	Remainder

The alloy was made from Al-20Cr master alloy, 99% purity K_2ZrF_9 salt, and 99.99% purity aluminum. The melting and holding temperature was 800°C, which is high enough to ensure that all the zirconium and chromium dissolved in the aluminum, but it is low enough to minimize oxidation and absorption of hydrogen gas by the melt. The melt was degassed with Ar by means of a rotary degasser prior to casting. The pouring temperature was approximately 780°C, which is above the liquidus temperature of the alloy.

The water-chilled mold shown schematically in Fig. 5 was designed to produce samples for measuring room and elevated temperature tensile properties. The mold is made of copper in order to achieve a high cooling rate. Five water channels are drilled in the mold walls to enhance heat extraction from the cast part. The shape of the cast part is a disk 1.25 cm in height and 5 cm in diameter, which can then be machined to make standard tensile test samples. The cooling rate was measured at 3 locations along the thickness of the cast part and it was found to be 160°C/s at the top, 60°C/s at the middle, and 28°C/s at the bottom. Specimens for measuring tensile properties were machined from the top part of

[1] Inductotherm model Power-Track 35-96, Inductotherm Corp., Rancocas, N.J.

the cast part where the cooling rate is in excess of 80°C/s. The specimens were aged in a tabletop electric box furnace that is accurate to within ±5°C.

Conventional transmission electron microscopy[2] (TEM) was performed on samples produced by thinning specimens of the alloy to perforation by means of a twinjet electro-polisher operating at 20 volts and using a 25 volume percent nitric acid in methanol solution that was maintained at -20°C.

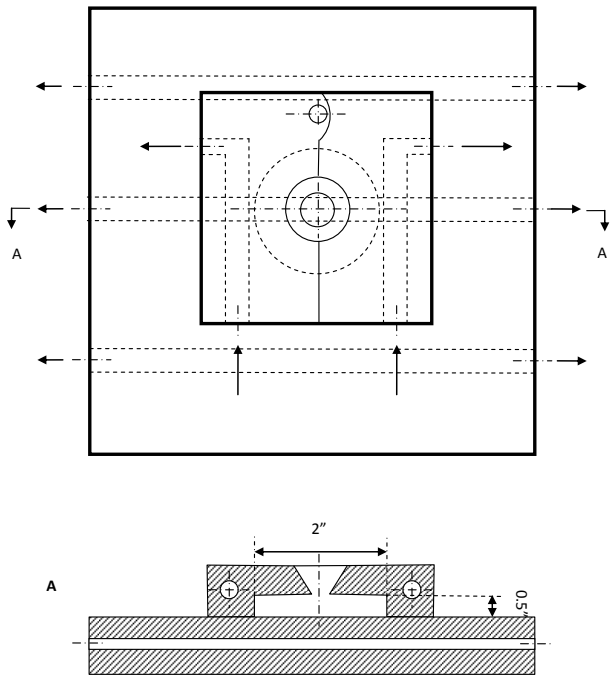

Fig. 5 Schematic representation of the water-chilled mold used to cast ingots from which samples were machined and used to measure tensile properties.

Room temperature tensile property measurements were performed according to ASTM standard B557 [41] on ASTM standard tensile specimens by means of a Universal Testing Machine[3]. Strain was measured by an axial extensometer[4] that has a maximum gage length of 5 cm. The extensometer was used until the

[2] JOEL 2010

[3] Instron Servo-hydraulic Tension-Compression System model 1332 equipped with an 8500 controller and a 5620 pound load cell.

[4] MTS extensometer model 634.25.

specimen fractured, and the testing machine ramp rate was 0.125 cm/min. Elevated temperature tensile property measurements were performed according to ASTM standard E21 [42] on ASTM standard tensile specimens by means of the same Universal Testing Machine and with the same strain rate. In this case, strain was measured by a high temperature axial extensometer[5] that has a maximum gage length of 2.5 cm; and here too, the extensometer was used until the specimen fractured. The specimens were heated to the test temperature, held at temperature until they equilibrated, and then tested to fracture in an environment chamber[6]. The chamber temperature did not vary from the set temperature by more than ±3°C. A minimum of 5 specimens were used in each test.

[5] MTS High Temperature extensometer model 633.11B-15.

[6] Instron Environment Chamber model 3116.

4. Results and Discussion

4.1 The Effect of Cooling Rate on the Formation of Primary Phases

In typical aluminum-transition metal systems, a high cooling rate is necessary to ensure formation of the supersaturated solid solution and prevent the formation of primary phases. However, the upper limit on cooling rate is about 100°C/s, which is the maximum cooling rate attainable by high-pressure die-casting. Hence, it is necessary to establish the critical cooling rate needed to avoid forming primary phases. Zirconium and Chromium have a larger atomic number than that of aluminum, which makes it possible to distinguish the primary phases by the Z-contrast in SEM Back Scattered Imaging Mode. Figs. 6 and 7 show the typical morphology of the primary Al_3Zr and $Al_{13}Cr_2$ phases, respectively. Fig. 8 shows images of the Al_3Zr primary phase in a binary Al-0.4Zr alloy that is cooled with different cooling rates. It is obvious from Fig. 8 that a higher cooling rate leads to less primary phases. It is estimated that the critical cooling rate for Al-0.4Zr binary alloy is around 55°C/s. However, in the Al-0.8Cr alloy, the primary $Al_{13}Cr_2$ phase forms even when the sample is cooled with a cooling rate of 90°C/s. Therefore, the critical cooling rate for the binary Al-0.8Cr alloy is in excess of 90°C/s.

Fig. 9 shows that in the ternary Al-0.8Cr-0.4Zr alloy, the Zr-containing primary phase and the Cr-containing primary phase can form separate from one another (Fig. 9(a)) and also they can form together (Fig. 9(b)). Fig. 10 shows a comparison of the critical cooling rates of the Al-0.4Zr, Al-0.8Cr and Al-0.8Cr-0.4Zr alloys. It is clear that the addition of Cr decreases the critical cooling rate of the Al-0.4Zr alloy significantly, which makes it easier to form a supersaturated solid solution in this alloy than in the binary alloys.

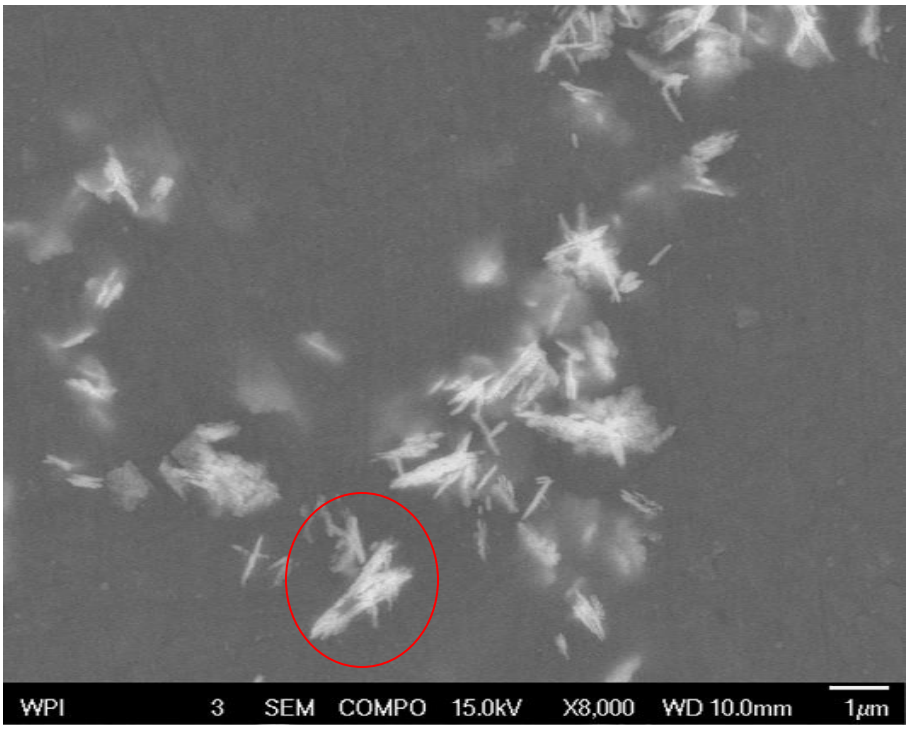

(a)

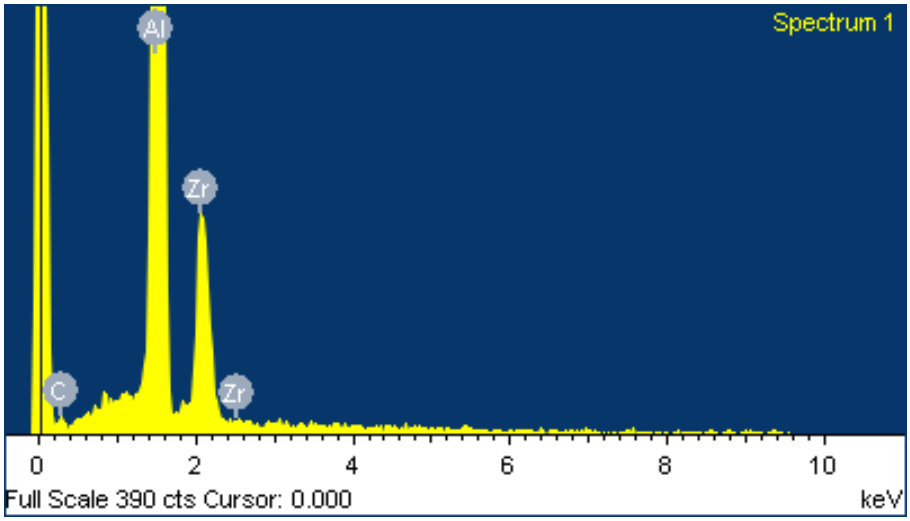

(b)

Fig. 6 (a) The morphology of Al_3Zr primary phase and (b) EDS from the particles in (a).

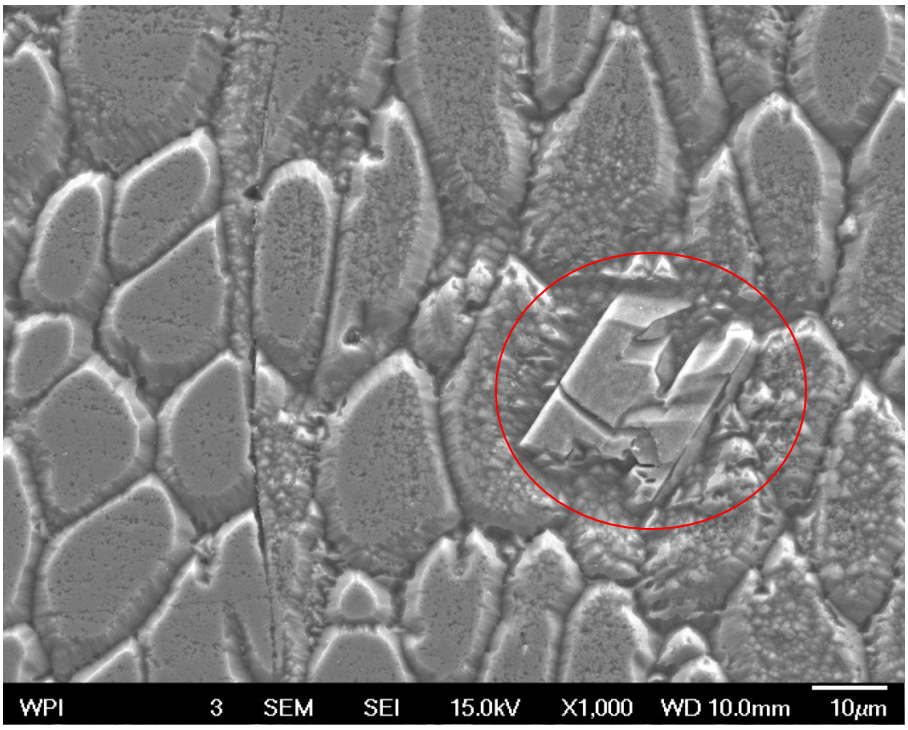

(a)

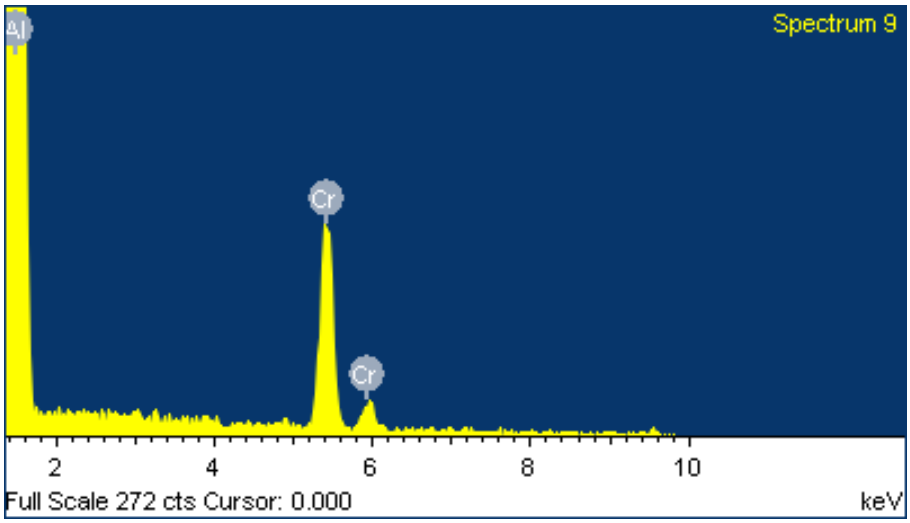

(b)

Fig. 7 (a) Morphology of primary $Al_{13}Cr_2$ phase and (b) EDS of the particle in (a).

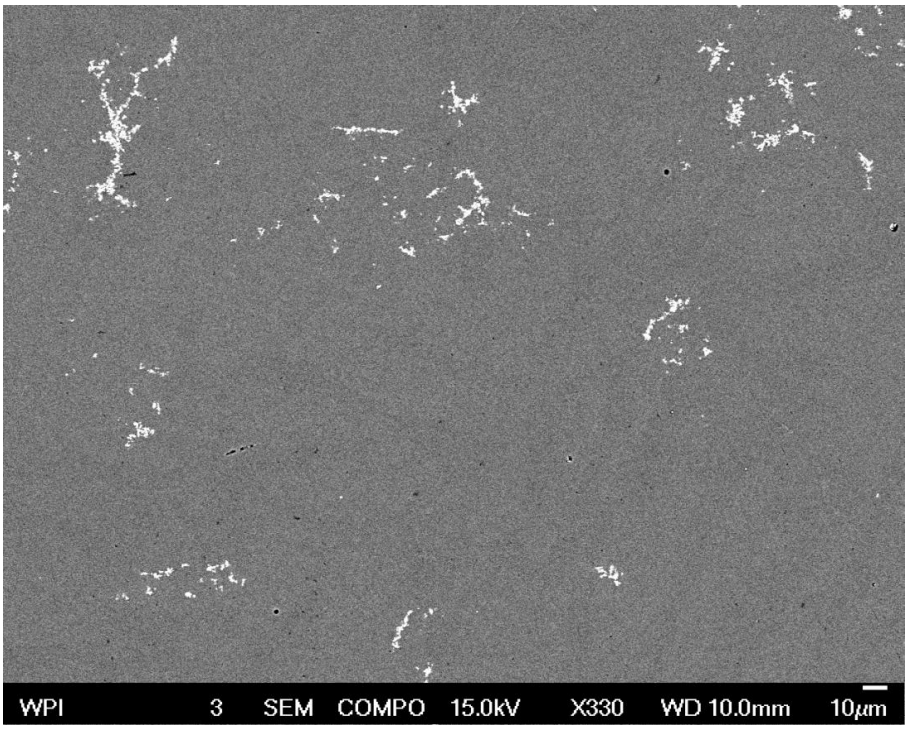
WPI 3 SEM COMPO 15.0kV X330 WD 10.0mm 10μm

(a)

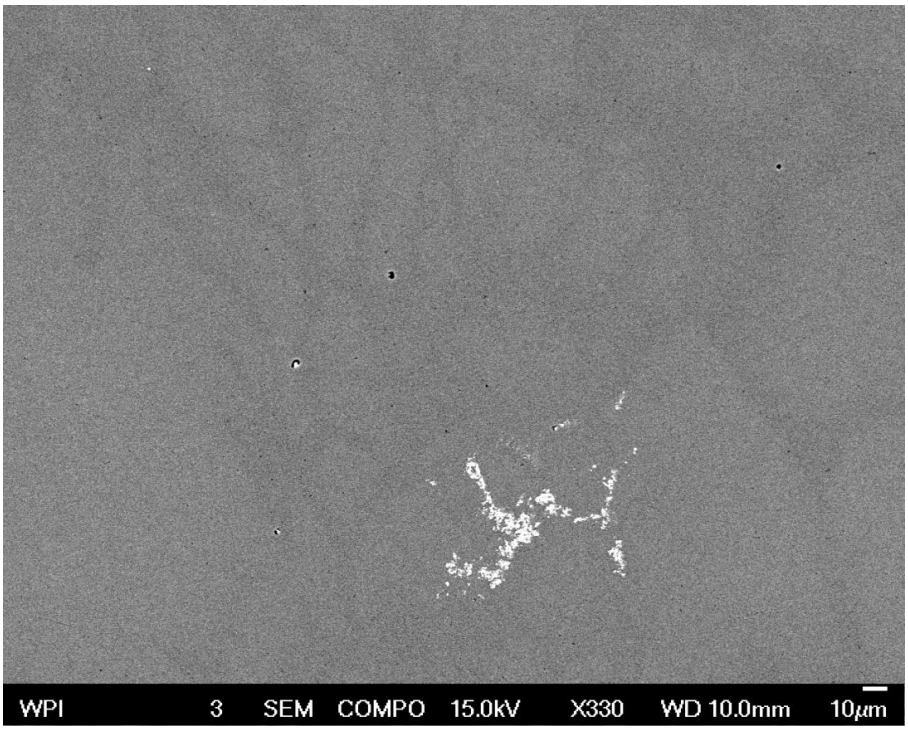
WPI 3 SEM COMPO 15.0kV X330 WD 10.0mm 10μm

(b)

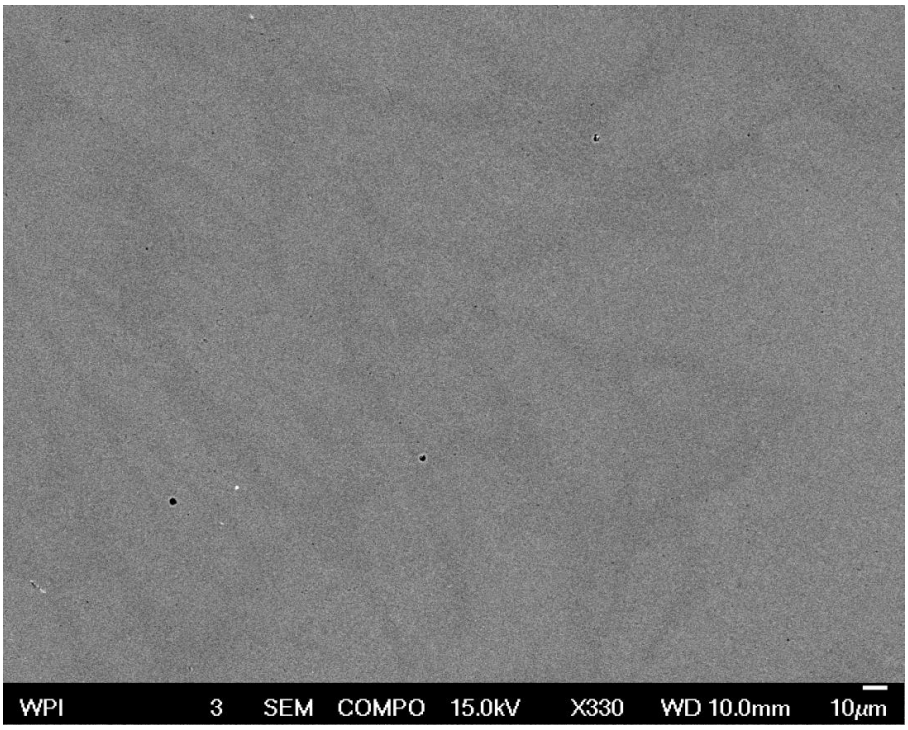

(c)

Fig. 8 Backscattered SEM images of the Al_3Zr primary phase in samples cooled with different cooling rates. (a) 10°C/s, (b) 40°C/s, and (c) 60°C/s.

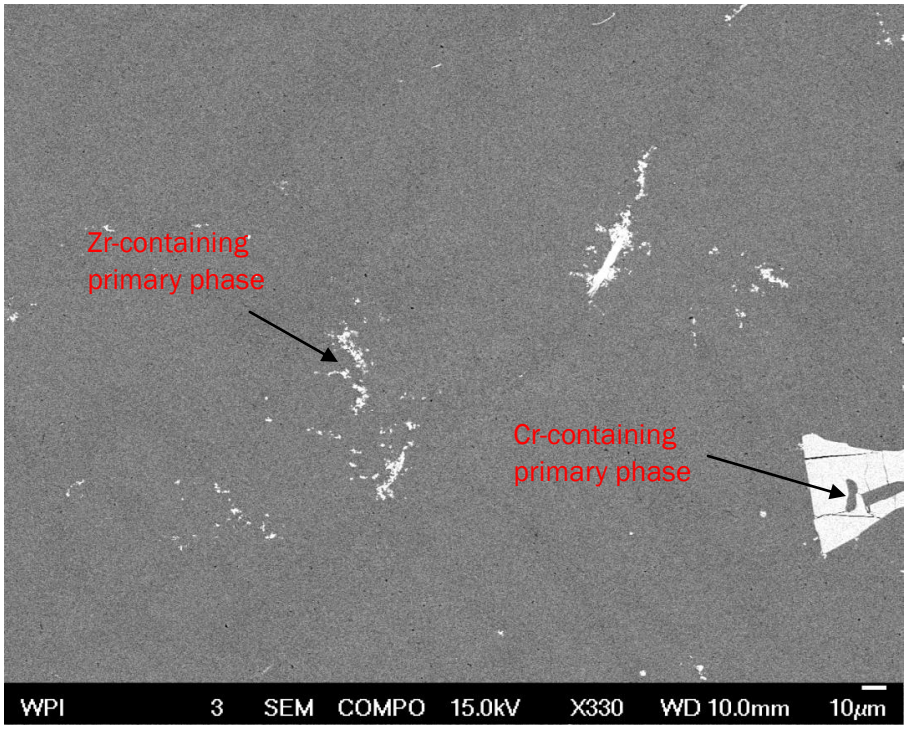

(a)

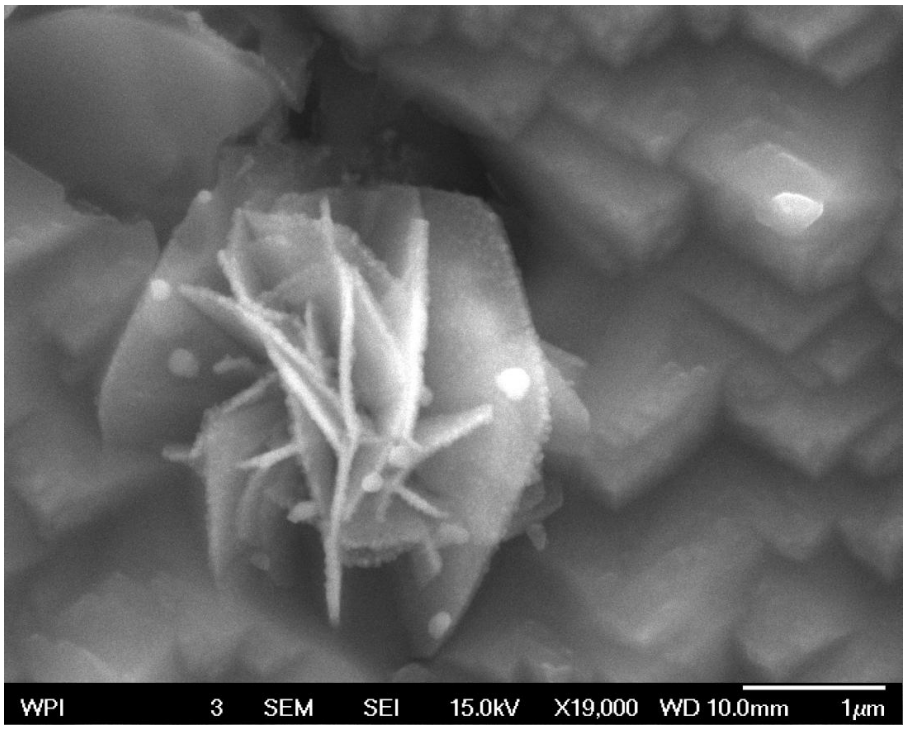

(b)

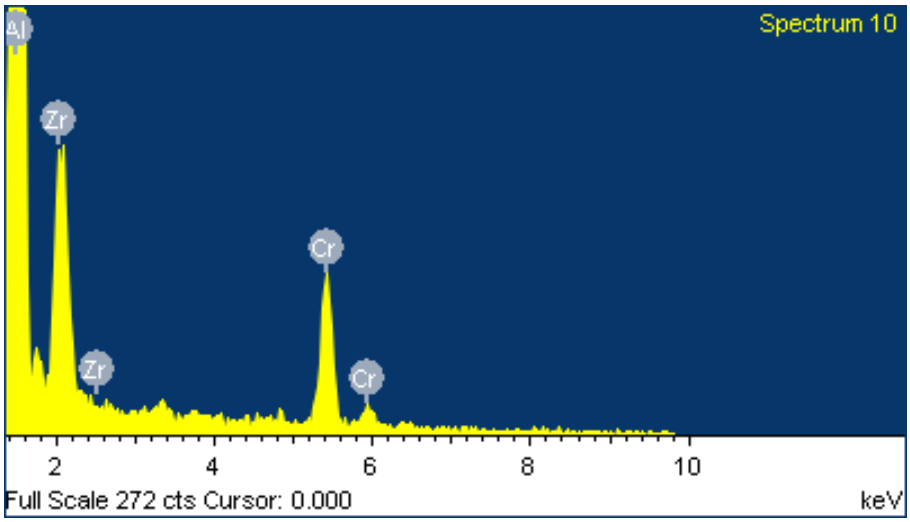

(c)

Fig. 9 SEM image of the ternary Al-0.8Cr-0.4Zr alloy (a) sample in which the Cr-containing primary phase and the Zr-containing primary phase form separately; and (b) sample in which the two phases form together. (c) EDS of the particle shown in (b).

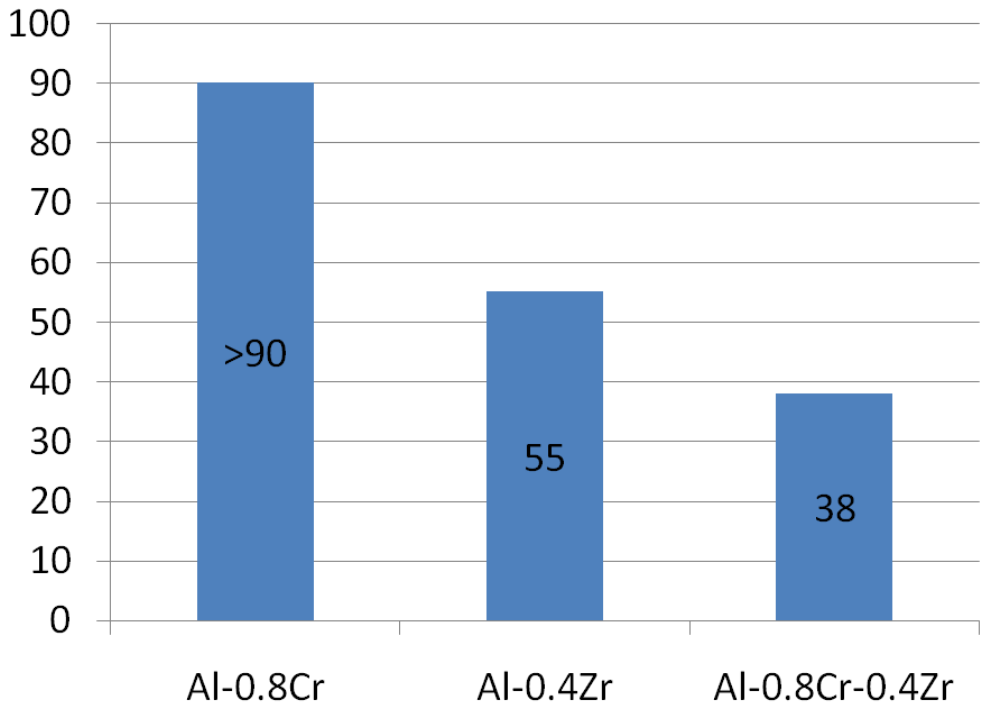

Fig. 10 The critical cooling rate of alloys with different chemical compositions.

4.2 Aging of Binary Al-Zr, Al-Cr, and Ternary Al-Zr-Cr alloys

4.2.1 One-Step Isothermal Aging

Al-0.4Zr binary alloy – The alloy was cooled at a rate of 90°C/s. As mentioned earlier, with such fast cooling rate the as-cast Al-0.4Zr alloy is a supersaturated solid solution. Samples of this supersaturated solid solution were aged at 400°C and also at 450°C. Fig. 11 shows the changes in Vickers microhardness of the alloy during isothermal aging for 3 hours, 6 hours, 12 hours, 24 hours and 48 hours. The Al-0.4Zr alloy is age-hardnable at 400°C and at 450°C and the metastable Al_3Zr precipitate is responsible for the increase in mcirohardness. The alloy reaches its peak microhardness of 35 HV_{200} when it is aged for 12 hours at 450°C. When the aging temperature is 400°C, the peak microhardness of 36.5 HV_{200} is obtained after 24 hours.

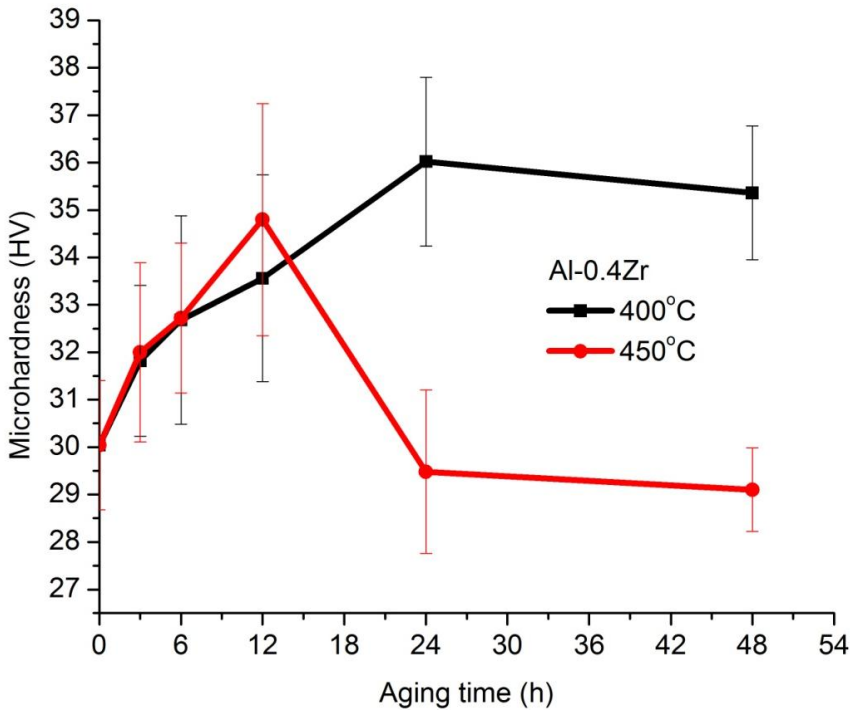

Fig. 11 Change in microhardness during isothermal aging of Al-0.4Zr alloy.

Al-0.8Cr binary alloy – The alloy was cooled at a rate of 90°C/s. As mentioned earlier, the critical cooling rate of the Al-0.8Cr alloy is in excess of 90°C/s. Hence, the Al-0.8Cr alloy does not form a supersaturated solid solution at this cooling rate. Specimens of this alloy were aged at 450°C for 3 hours, 6 hours, 12 hours, 24 hours, and 48 hours. The change in Vickers microhardness during isothermal aging of the Al-0.8Cr alloy at 450°C is shown in Fig. 12. Fig. 12 shows that the microhardness of the alloy decreases from 48 HV_{200} to 32 HV_{200} after aging for 48 hours at 450°C. During aging, the primary $Al_{13}Cr_2$ phase grows and causes this decrease in microhardness.

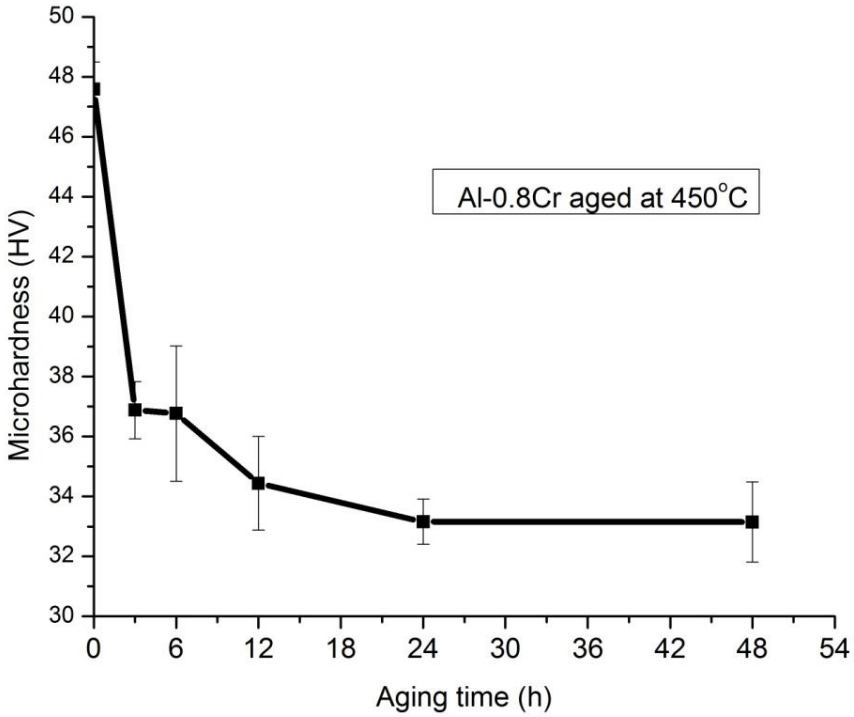

Fig. 12 Change in microhardness during isothermal aging of Al-0.8Cr alloy at 450°C.

Al-0.4Zr-0.4Cr ternary alloy – With a cooling rate of 90°C/s, the ternary Al-0.4Zr-0.4Cr as-cast alloy is a supersaturated solid solution. The change in Vickers microhardness of the alloy when aged at 400°C and at 450°C is shown in Fig. 13. The Al-0.4Zr-0.4Cr alloy is age-hardnable at these two temperatures. When the aging temperature is 400°C, the microhardness of the Al-0.4Zr-0.4Cr alloy reaches its peak value of 45 HV_{200} after aging for 24 hours. When aged at 450°C, the microhardness of the Al-0.4Zr-0.4Cr alloy reaches its peak value of 40 HV_{200} after aging for only 6 hours. This is similar to the case of the binary Al-0.4Zr where aging at the higher temperature requires less time for the alloy to reach peak hardness, whereas aging at the lower temperature takes longer but results in higher peak hardness. Fig. 14 shows a comparison of the Vickers microhardness of the binary Al-0.4Zr and the ternary Al-0.4Zr-0.4Cr both aged at 400°C. The two alloys achieve their highest hardness at this temperature when they are aged for 24 hours. The introduction of Cr significantly increases the microhardness of the

binary Al-0.4Zr alloy. The Vickers microhardness increases about 40%, from 37 HV_{200} to 45 Hv_{200}.

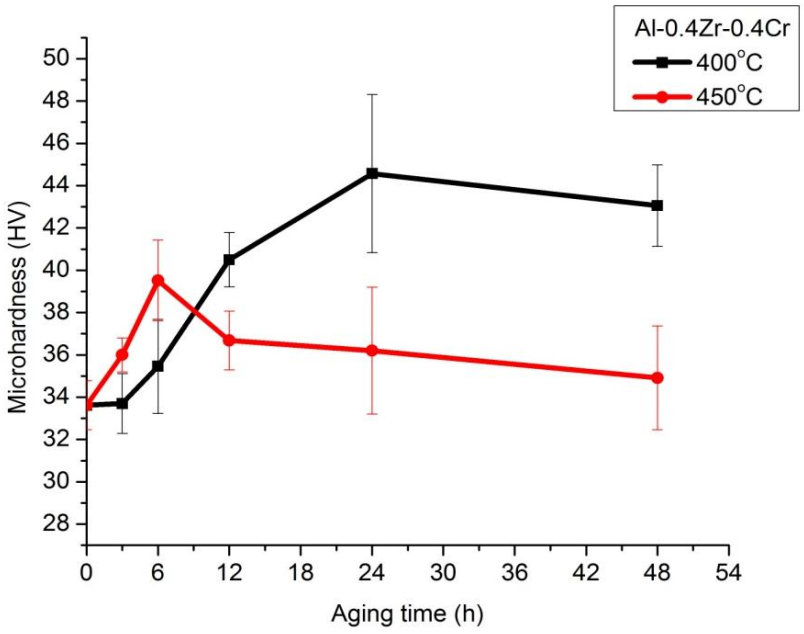

Fig. 13 Change in microhardness during isothermal aging of Al-0.4Zr-0.4Cr.

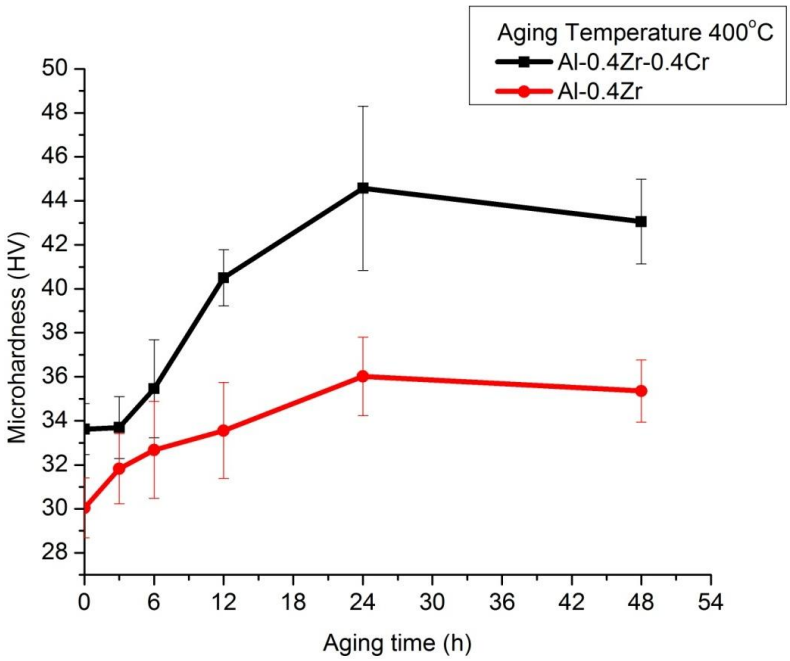

Fig. 14 Comparison of the microhardness of Al-0.4Zr and Al-0.4Zr-0.4Cr alloys.

Al-0.4Zr-0.8Cr ternary alloy – With a cooling rate of 90°C/s, the ternary Al-0.4Zr-0.4Cr as-cast alloy is a supersaturated solid solution. The change in Vickers microhardness of the alloy when aged at 400°C and at 450°C is shown in Fig. 15. The Al-0.4Zr-0.8Cr alloy reaches its peak microhardness of 57 HV_{200} when it is aged at 400°C for 24 hours. When the aging temperature is 450°C, the microhardness reaches its peak value of 49 HV_{200} when the alloy is aged for 12 hours. Fig. 16 is a comparison of the microhardness of the ternary Al-0.4Zr-0.8Cr and the binary Al-0.8Cr and Al-0.4Zr alloys all aged at 450°C. Compared to the binary Al-0.4Zr and Al-0.8Cr alloys, the ternary Al-0.4Zr-0.8Cr alloy has several advantages: It is age-hardnable while the binary Al-0.8Cr alloy is not, and it has a higher hardness than the binary Al-0.4Zr alloy.

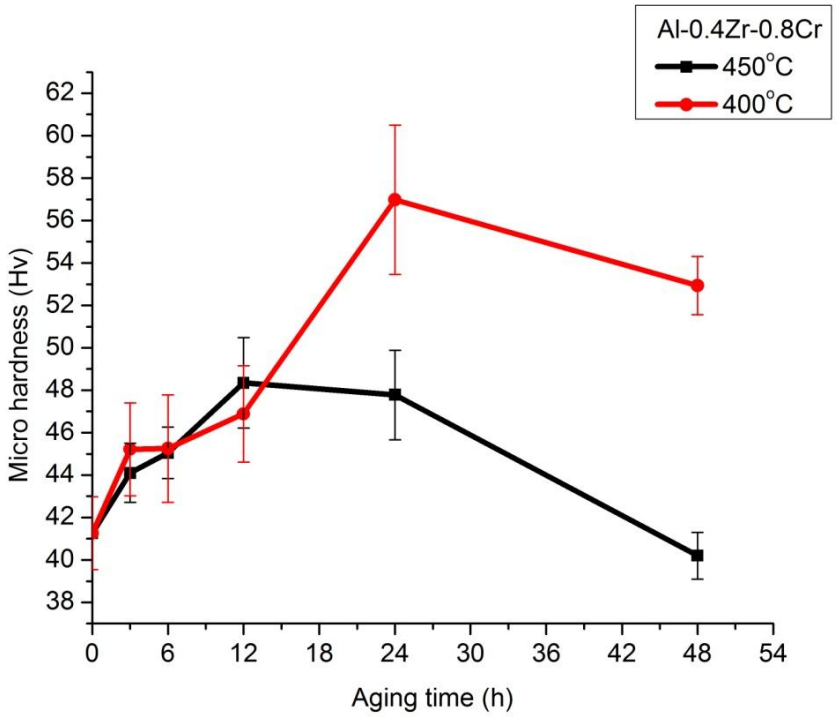

Fig. 15 Change in microhardness during isothermal aging of Al-0.4Zr-0.8Cr.

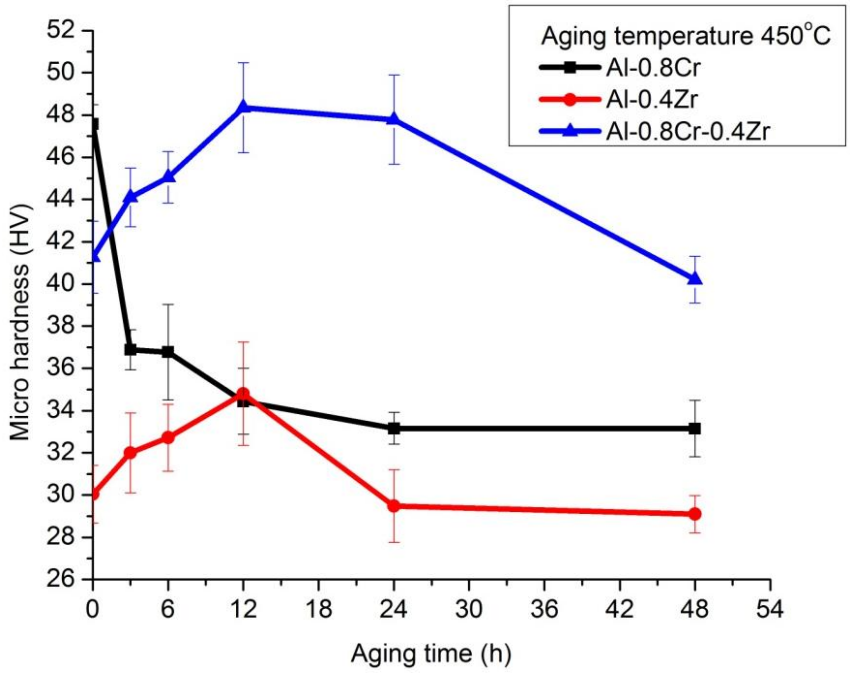

Fig. 16 Comparison of the microhardness of Al-0.4Zr, Al-0.8Cr, and Al-0.4Zr-0.8Cr alloys.

4.2.2 Two-Step Isothermal Aging

In addition to traditional one-step isothermal aging, the Al-0.4Zr-0.8Cr alloy was also aged isothermally in two steps wherein the specimens are held at 375°C for three hours, and then at 425°C for either 3 hours, 6 hours, 12 hours, 24 hours, or 48 hours. Fig. 17 shows the changes in Vickers microhardness of the alloy during the two-step isothermal aging. Compared with traditional one-step isothermal aging at 400°C, the two- step isothermal aging increases the peak microhardness from 57 HV_{200} to 59 HV_{200}. However, with the two-step aging process, the microhardness reaches a stable value after 6 hours (with variation between $55Hv_{200}$ and $59HV_{200}$). This suggests that two-step isothermal aging can be used to shorten the aging time of this alloy. The low first aging temperature (375°C) allows more particles to precipitate, which leads to a higher peak microhardness and the higher second aging temperature (425°C) accelerates the precipitation process and reduces the overall aging time.

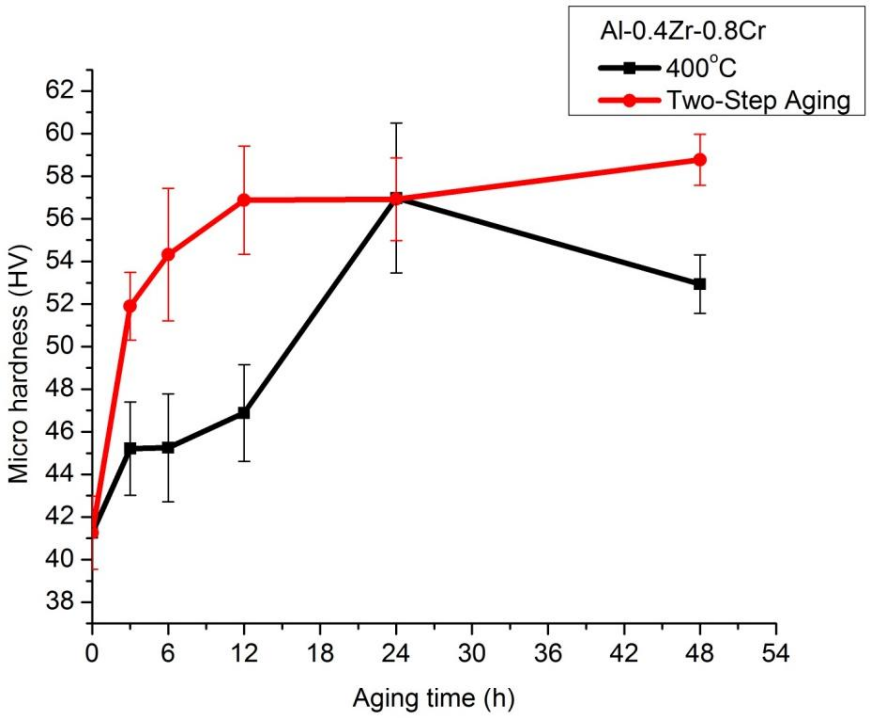

Fig. 17: Change in microhardness during two-step isothermal aging of Al-0.4Zr-0.8Cr alloy.

4.3 Room and Elevated Temperature Tensile Properties of Al-Zr-Cr Alloys

Fig. 18 shows a typical stress-strain curve of Al-0.4Zr-0.8Cr alloy at room temperature and at 300°C. Prior to testing, the alloy is aged at 400°C for 24 hours. The yield stress of the alloy at room temperature and at 300°C is 10.5 ksi and 5.9 ksi, respectively. Fig. 19 shows a comparison of the stress-strain curves for the alloy tested at 300°C for samples that were aged according to a one-step isothermal schedule and a two-step isothermal schedule. With two- step isothermal aging, the yield stress increases from 5.9 ksi to 6.3 ksi after 15 hours (3 hours at 375°C and 12 hours at 425°C). Fig 20 shows the variation in the yield stress at 300°C as function of the temperature of step 2 of the isothermal two-step aging schedule. Fig. 20 shows that the aging time has little effect on high temperature yield stress. Fig. 21 shows a comparison between commercial A390 alloy and Al-0.4Cr-0.8Cr alloy. The yield strength of the Al-0.4Zr-0.8Cr alloy is about 60% that of the A390 alloy.

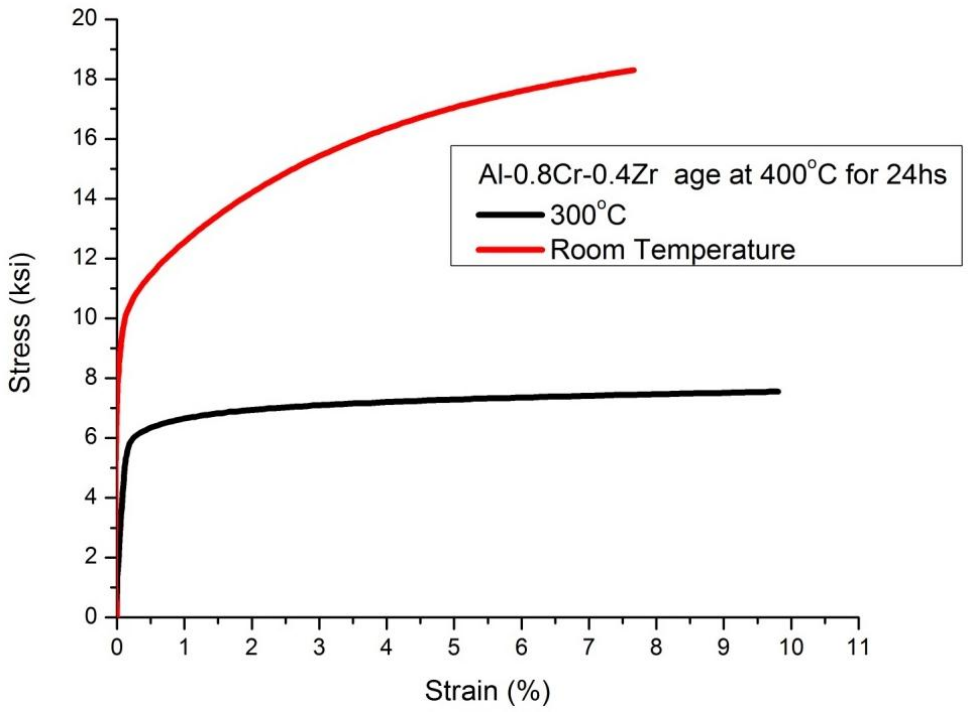

Fig. 18 Stress-strain curve of Al-0.4Zr-0.8Cr alloy at room temperature and at 300˚C.

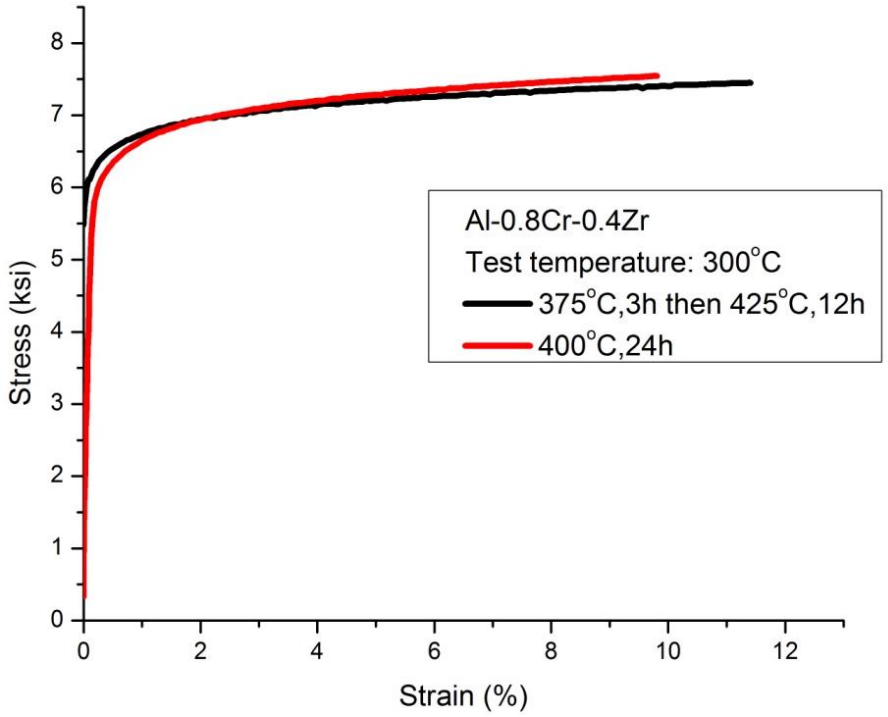

Fig. 19 Stress-strain curves of alloys aged with different schedules.

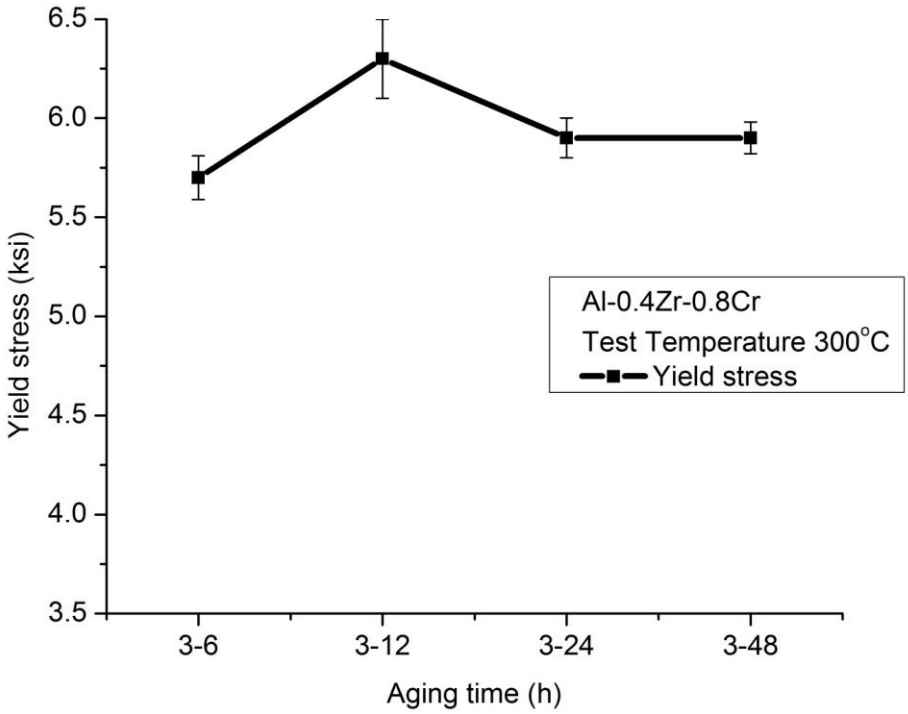

Fig. 20 Yield stress at 300˚C as function of the temperature of step 2 in an isothermal two-step aging process.

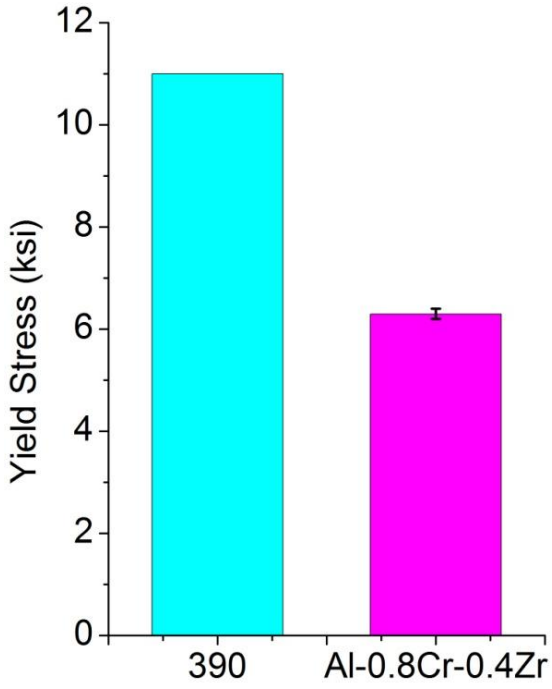

Fig. 21 Yield strength at 300°C of A390 and Al-Zr-Cr alloys.

4.4 Thermal Stability of Al-Zr-Cr Alloys

Al-0.4Zr-0.8Cr alloy specimens that were aged for 24 hours at 400°C were soaked at 300°C for 100 hours in order to simulate use at elevated temperature. Fig. 22 shows that the alloy loses only a little of its yield strength after been soaked at 300°C for 100 hours. Fig. 23 shows the yield stress at 300°C of alloy samples that were held for 100 hours at 450°C. After this long time at the high temperature, the alloy has good strength. The slight decrease in strength reflects the slow coarsening behavior of the strengthening particles. From Figs. 22 and 23, it is seen that Al-Zr-Cr alloys are thermally stable when used at temperatures up to 300°C and are only slightly affected by higher temperatures (up to 450°C).

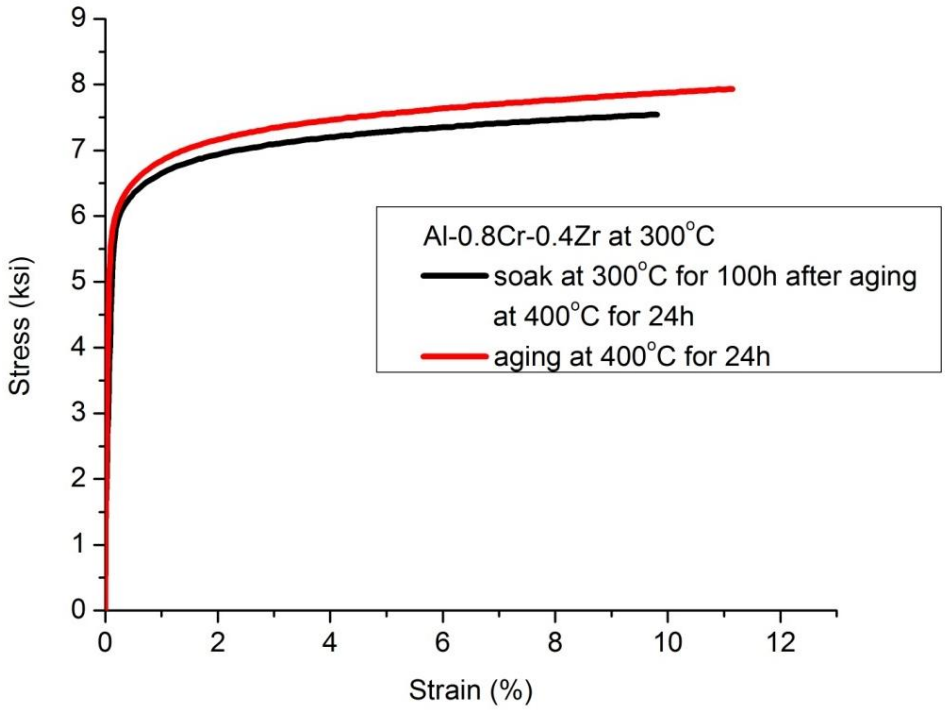

Fig. 22 Stress-strain curve of Al-0.4Zr-0.8Cr alloy soaked at 300˚C for 100h.

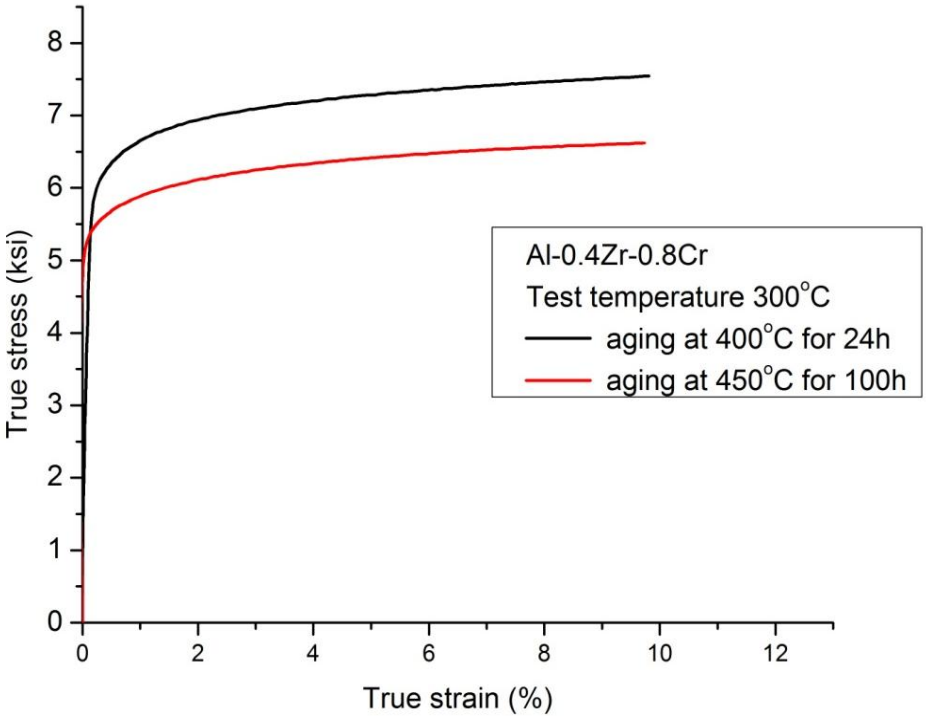

Fig. 23 Stress-strain curve of Al-0.4Zr-0.8Cr aged for 100h at 450˚C.

4.5 Chemical Composition and Crystal Structure of the Precipitates

Fig. 24 and 25 show TEM images of the precipitates that form in Al-0.4Zr-0.8Cr alloy. This sample was aged at 450°C for 100 hours in order to coarsen the particles and make them easier to identify. After this treatment, the mean radius of the particles is 30 nm. From the diffraction pattern, it is clear that the precipitate has an $L1_2$ crystal structure and that the particles are coherent with the aluminum matrix.

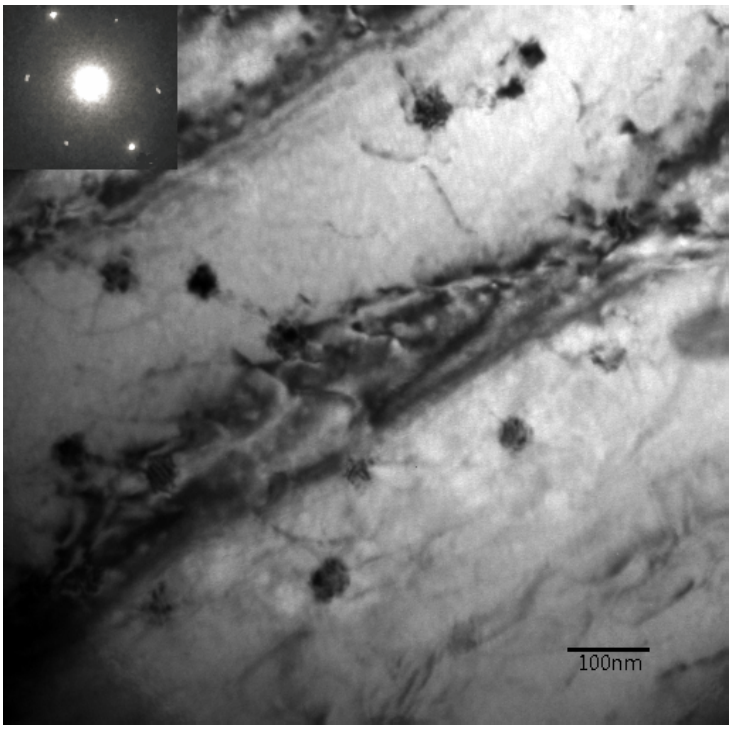

Fig. 24 TEM image of the precipitates in Al-0.4Zr-0.8Cr alloy. The sample was tilted to the [110] zone axis.

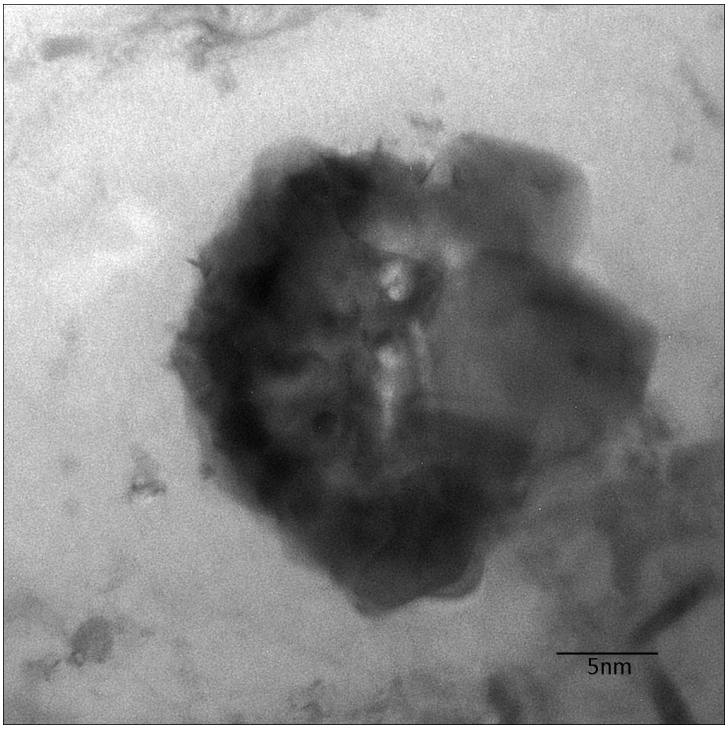

Fig. 25 High magnification image of the particle in Fig. 24.

Fig. 26 is an EDS chart of a typical precipitate particle in the Al-0.4Zr-0.8Cr alloy. It is clear that the particle has a significantly higher Zr content than the matrix. On the other hand, the intensity of Cr is unchanged between the particle and the matrix. This indicates that Zr is an ingredient of the precipitate while Cr is present only in the matrix. Accordingly, it is suggested that two mechanisms contribute to the strength of the Al-0.4Zr-0.8Cr alloy when it is quenched from the melting temperature at a rate of 90°C/s and aged at 450°C for 100 hours: Cr forms a solid solution with the α-aluminum giving rise to solid solution strengthening; and Zr-containing precipitate particles form and give rise to precipitation hardening. With the help of EDS and the Cliff-Lorimer equation, it is possible to determine the chemical composition of the precipitate. The Cliff-Lorimer equation [43] is shown as Eq. (8) in which C_A is the weight percent of element A, C_B is the weight percent of element B; k_{AB} is the Cliff-Lorimer factor, and I is the peak intensity.

$$\frac{C_A}{C_B} = k_{A-B}\frac{I_A}{I_B} \tag{8}$$

With Eq. (8), the ratio of the weight percent zirconium to the weight percent aluminum in the precipitate particle (i.e., C_{Zr} and C_{Al}) is determined as follows:

$$\frac{C_{Zr}}{C_{Al}} = k_{Zr-Al}\frac{I_{Zr}}{I_{Al}} = 2.17 \times \frac{9.9}{18.3} = 1.17$$

And the ratio of the atom percent zirconium to the atom percent aluminum in the precipitate particle (i.e., Zr_{atom} and Al_{atom}) is determined as follows:

$$\frac{Zr_{atom\,\%}}{Al_{atom\,\%}} = \frac{\left(\frac{C_{Zr}}{C_{Al}}\right)}{\left(\frac{M_{Zr}}{M_{Al}}\right)} = \frac{1}{2.9} \cong \frac{1}{3}$$

Therefore, the precipitate is metastable Al_3Zr particles that have the $L1_2$ crystal structure.

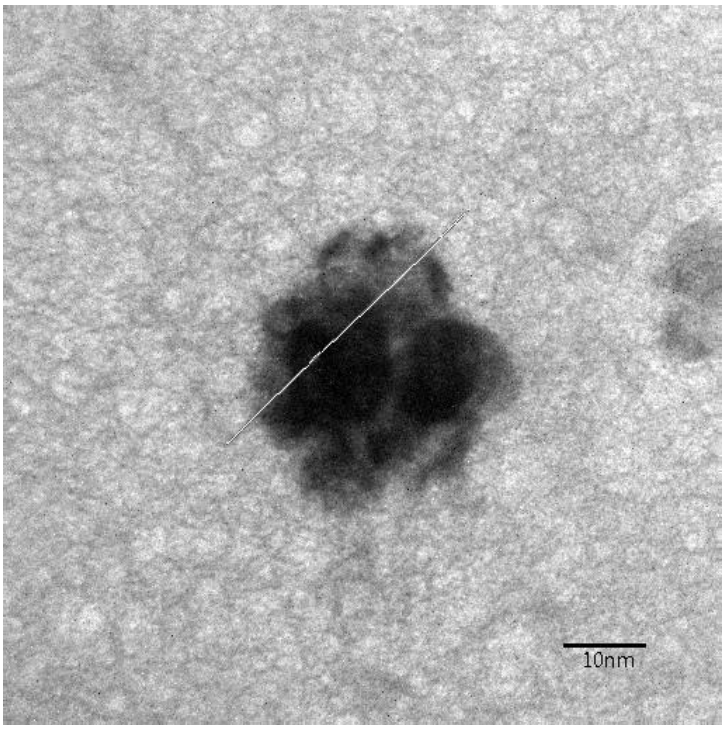

(a)

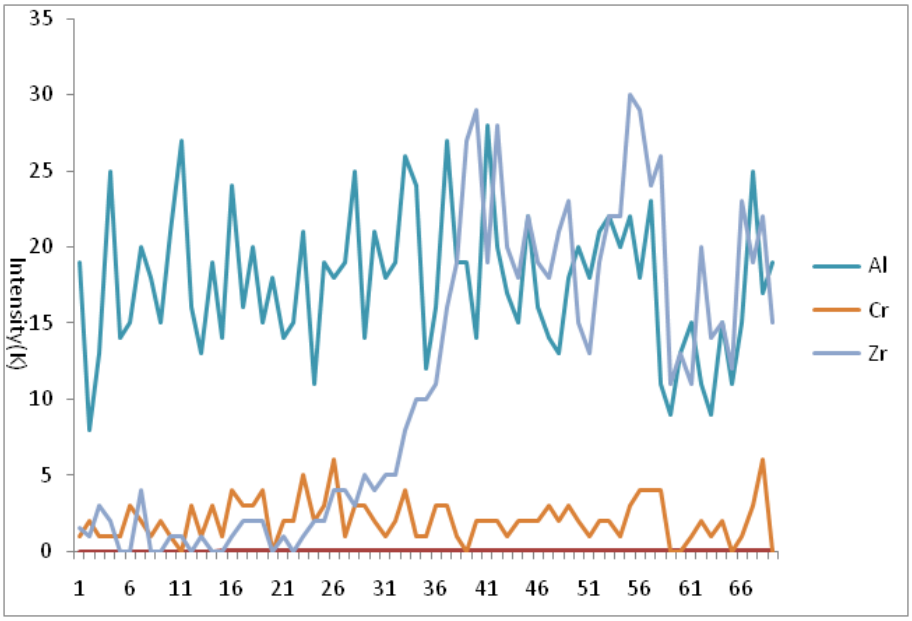

(b)

Fig. 26 EDS of a typical precipitate particle in the Al-0.4Zr-0.8Cr alloy.

5. Conclusions and Suggested Future Work

1. The addition of chromium to Al-Zr binary alloys significantly decreases the alloy's critical cooling rate. The critical cooling rate of Al-0.4Zr and Al-0.4Zr-0.8Cr alloys is measured to be 55°C/s and 38°C/s, respectively.
2. Two strengthening mechanisms function in quenched and aged Al-Zr-Cr alloys. Cr atoms remain in the matrix during aging and lead to solid solution strengthening. On the other hand, Zr forms Al_3Zr precipitate particles. The Al_3Zr particles are metastable and have the $L1_2$ crystal structure. They strengthen the alloy by precipitation hardening.
3. The Al-0.4Zr-0.8Cr alloy is stable at 300°C and its yield strength after soaking for 100 hours at 300°C is 6 ksi.
4. The yield strength of the Al-0.4Zr-0.8Cr alloy is only 60% that of commercial A390 alloy. It is suggested that future work should focus on adding other transition elements (either ones that form precipitates with aluminum, or ones that form solid solution with aluminum) to the Al-0.4Zr-0.8 alloy in order to increase its strength. Furthermore, a eutectic system, such as Al-Fe or Al-Ni, may be added to the Al-0.4Zr-0.8Cr alloy in order to improve its castability.

References

1. E. O. Hall, Pro. Phys. Soc. London, B64, 1951, p. 747.
2. N. J. Petch, J. Iron and Steel Inst., 174, 1953, p. 25.
3. Michael T. Stawovy, 1998, Processing of Aluminum Alloys Containing Displacement Reaction Products. Ph.D thesis, Virginia Polytechnic Institute and State University.
4. E. Orowan: 'Internal stress in metals and alloys,' 451; 1948, London, The Institute of Metals.
5. P. Hirsch, F. Humphreys, in: A.S. Argon (ed.), Physics of strength and plasticity. MIT Press, Cambridge, MA (1969) 189.
6. A.J. Ardell: Metal Trans A 16 (1985) 2131.
7. E. Nembach: Particle Strengthening of Metals and Alloys. John Wiley & Sons, New York (1997).
8. A. Ardell, in: J.H. Westbrook, R.L. Fleischer(Eds.), Intermetallic Compounds: principles and Practice, Vol. 2. John Wiley & sons (1994) 257.
9. Ham RK. 3rd Bolton Landing Conference, Kear BH., Sims CT., Stoloff NS., Westbrook JH., editors, 1969; p365.
10. Lifshitz, I.M. and Slyozov, V.V., J. Phys. Chem. Solids, 1961. 19: p. 35.
11. Wagner, C., Z. Elektrochemie, 1961. 65: p. 581.
12. Wagner, R., Kampmann, R., and Voorhees, P., Homogeneous Second-Phase Precipitation, in Phase Transformations in Materials, Kostorz, G., Editor. 2001, Wiley-VCH: New York. p. 309.
13. Ratke, L. and Voorhees, P.W., Growth and Coarsening: Ripening in Materials Processing. 2002, Berlin: Springer Verlag.
14. H.A. Calderon, P.W. Voorhees, J.L. Murray, G. Kostorz: Acta Metall. Mater. 42 (1994) 991.
15. Knipling KE, Dunand DC, Seidman DN. Z Metallkd 2006;97:246–65.

16. N. Ryum, Acta. Metall. 17 (1969) 269.

17. Keith E. Knipling, David C. Dunnand, Acta. Mater., 58 (2008) 1182.

18. American Society for Metals, Metal Handbook, Vol.8, 8th ed., p 265, ASM international, Materials Park, OH (1973).

19. M.S. Zedalis, M.E. Fine, Metall. Trans. A, 17 (1986) 2187.

20. Won-Wook Park, Mater. and Design. 17 (1996) 85.

21. Y.C. Chen, M.E. Fine, Acta. Metall. 38 (1990) 771.

22. Keith E. Knipling, David C. Dunand, Acta. Mater. 56 (2008) 114.

23. Chun-Huei Tsau, Yen-Cheng Chen, Mater. Phy. and Chem. 73 (2002) 111.

24. S.P. Wen, K.Y. Gao, Scripta Mater. In Press.

25. Christan B. Fuller, David N. Seidman, David C Dunand, Acta. Mater. 51 (2003) 4803.

26. N.A. Belov, A.N. Alabin, D.G. Eskin, J. Mater. Sci. 41 (2006) 5890.

27. Keith E. Knipling, Richard A. Karnesky, Acta. Mater. 58 (2010) 5184.

28. W. Lefebvre, F. Danoix, J. Alloys and Compounds 470 (2009) 107.

29. O.N. Senkov, M.R. Shagiev, Acta. Mater. 56 (2008) 3723.

30. A. Tolley, V. Randmilovic, Scripta Mater. 52 (2005) 621.

31. Christian B. Fuller, Joanne L. Muarry, Acta. Mater. 53 (2005) 5401.

32. B. Forbord, W. Lefebvre, Scripta Mater. 51 (2004) 333.

33. H. Hallem, W. Lefebvre, Mater. Sci. and Eng. A 421 (2006) 154.

34. P.B. Desch, R.B. Schwarz, P. Nash: J. Less-Common Metals 168 (1991) 69.

35. K.I. Moon, K.Y. Chang, K.S. Lee: J. Alloys Compounds 312 (2000) 273.

36. K.I. Moon, S.C. Kim, K.S. Lee: Intermetallics 10 (2002) 185.

37. L. Bendersky, R. J. Schaefer, F. S. Biancaniello, D. Shechtman: Journal of Materials Science 21 (1986) 1892.

38. G. J. Marshall, I. R. Hughes and W. S. Miller, Mat. Sci. Technol., 2 (1986) 394.

39. American Society for Metals, Metal Handbook, Vol.8, 8th ed., p 258, ASM international, Materials Park, OH (1973).

40. Ternary Phase Diagram For Al-Zr-Cr. (2012). Retrieved December 6, 2012, from http://www.springermaterials.com/docs/VSP/datasheet/lpf-c/00951000/LPFC_951370.html.

41. ASTM Standard B557 "Standard Methods of Tension Testing Wrought and Cast Aluminum and Magnesium Alloy Products", Annual Book of ASTM Standard, Vol. 02.02, 1993.

42. ASTM Standard E21 "Elevated Temperature Tensile Test of Metallic Materials", Annual Book of ASTM Standaard, Vol. 03.01, 1993.

43. B. Fultz, J. M. Howe, Transmission Electron Microscopy and Diffractometry of Materials, 2nd ed., p 214, Springer-Verlag Berlin Heidelberg, New York, NY (2002).